Surface Review and Letters, Vol. 18, No. 6 (2011) 289−296

DOI: 10.1142/S0218625X11014771

World Scientific
www.worldscientific.com

THERMAL MODEL FOR LASER-INDUCED DISCHARGE SURFACE STRENGTHENING

ZHONGQIANG ZHOU*, ZHITONG WANG and MINGJIANG YANG
Key Lab of Mechanics in Advanced Manufacturing,
Institute of Mechanics Chinese Academy of Sciences,
Beijing 100190, China
**zhouzhongqiang@gmail.com*

Received 3 May 2011

The temperature field due to laser-induced discharge surface strengthening (LIDSS) has significant influence on the microstructure transformation and also the formation quality of discharge pit. A transient axisymmetric thermal model is developed to estimate the temperature distribution during LIDSS based on Fourier heat conduction equation. In the model, a Gaussian heat input distribution is assumed; temperature-dependent material properties are applied and the latent heat of fusion and vaporization is calculated on an enthalpy method. As an application, we use this model to compute the temperature field during the process of tungsten tool electrode machining 1045 steel workpiece and find that the computational results are well consistent with the experimental data.

Keywords: Laser-induced discharge; surface strengthening; thermal model; heat source.

1. Introduction

Laser-induced discharge surface strengthening (LIDSS) is a novel discrete-strengthening technology which utilizes small energy pulsed laser to trigger and induce discharge between two electrodes — the tool and the workpiece. During the LIDSS process, short-pulse laser about a few microseconds irradiates the surface of workpiece and makes the local irradiation area ionize rapidly and form the plasma plume which can guide the discharge process between anode and cathode. Laser-induced discharge surface strengthening is undeniably a thermal process where thermal energy is generated in a discharge channel and causes the work material to melt and even evaporate. As the discharge is completed, the discharge pit cools off rapidly and resolidifies into bright layer with high hardness on machined surface.

Compared with conventional electrical discharge machining (EDM),[1−3] LIDSS has longer single pulse duration and higher discharge energy. The former involves the material removal process,[4,5] while the latter involves the melting and resolidification process of material. As a new method of surface strengthening, there has been little research on LIDSS in literature available. Li *et al.*[6,7] investigated on morphology and depth of heat affected zone of discharge pit by high repetitive rate YAG laser-induced discharge, and concluded that morphology and depth of the heat affected zone are mainly determined by electrical polarity, medium and discharge parameters. Wang *et al.*[8] studied the effect of surface condition of electrode on surface melting of material by YAG laser-induced discharge. Recently, Wang and his co-workers[9] compared several discharge areas by laser-induced discharge and common arc discharge, and found that laser guidance controls the stochastic movement of the anode spot and avoids the repetitive melting and tempering microstructures in the discharge. However, no work has been done on the thermal model of LIDSS which is responsible for the microstructure transformation and formation quality of discharge pit.

In this paper, a transient axisymmetric thermal model for LIDSS is presented based on Fourier heat conduction equation. The principal aim of developing this model is to predict the temperature distribution during LIDSS as well as the diameter of discharge pit and the depth of hardened layer.

2. Experimental Procedure

We conducted the LIDSS experiments where YAG laser was used to induce tungsten cathode to discharge and machine 1045 steel anode (Fig. 1). The discharge current intensity ranged from 40 to 160 A and the current waveform was rectangular. The discharge pulse durations ranged from 0.5 to 10 ms with the pulse energy of 1.0 and 20 J. For each combination of current intensity and pulse duration, various diameters of discharge pit and the depths of hardened layer can be obtained. The diameter and depth were measured as Fig. 2. The experimental conditions are indicated in Table 1.

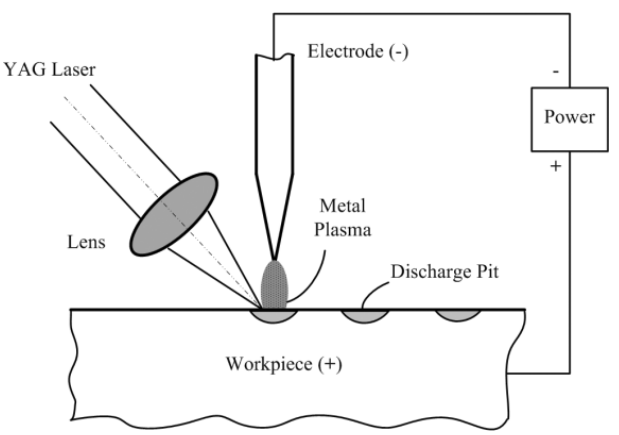

Fig. 1. Schematic of LIDSS.

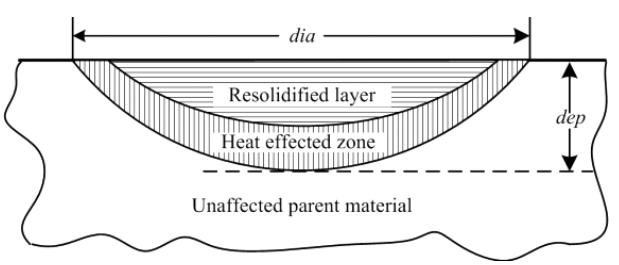

Fig. 2. The diameter (dia) of discharge pit and the depth (dep) of hardened layer.

Table 1. Experimental conditions.

Laser parameters	YAG laser, wavelength 1.06 μm, Spot radius 80 μm Pulse duration 600 ns, Pulse energy 25 mJ
Discharge parameters	1045 steel workpiece (+), tungsten electrode (−), Electrode spacing 0.5 mm, Current intensity 40 A to 160 A, Rectangular current waveform, pulse duration 0.5 ms to 10 ms, pulse energy 1.0 J to 20.0 J

3. Mathematical Modeling

Laser-induced discharge surface strengthening is complex and involves laser treatment of material and gas discharge, so the following assumptions are made to simplify the mathematical model.

3.1. *Assumptions*

- The domain is considered as axisymmetric.
- The workpiece is homogeneous and isotropic.
- The small energy of laser is neglected.
- The heat causing work material to melt and evaporate mainly comes from surface heat source formed during discharge.
- The thermal process is divided into two stages: heating and cooling. In the heating stage, radiation and convection heat losses are negligible whereas not in the cooling.
- The heat flux of heat input is assumed to obey Gaussian distribution.
- The analysis is done for a single discharge.

3.2. *Governing equation*

A simplified case is shown in Fig. 3, where a semi-infinite body is being heated by Gaussian heat source. Heating of workpiece due to a single discharge is assumed as axisymmetric, dependent on the following thermal diffusion differential equation.

$$\lambda\left\{\frac{1}{r}\frac{\partial}{\partial r}\left(r\frac{\partial T}{\partial r}\right)+\frac{\partial}{\partial z}\left(\frac{\partial T}{\partial z}\right)\right\}=\rho c\frac{\partial T}{\partial t}+\frac{\partial H}{\partial t}. \quad (1)$$

Here, T is temperature, t is time, λ is thermal conductivity, ρ is density, C is specific heat capacity,

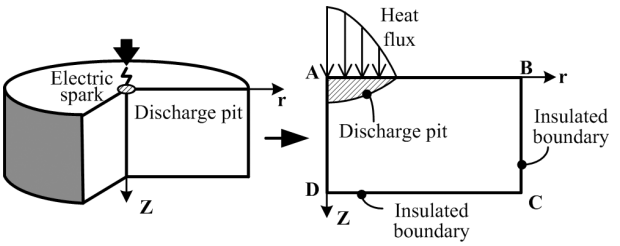

Fig. 3. Axisymmetric model and boundary conditions for solution.

H is the volumetric enthalpy of material (J/m^3) and r and z are coordinate axes (Fig. 3). In Eq. (1), the thermophysical properties λ, ρ, C and H may be highly dependent on temperature.

3.3. *Boundary and initial conditions*

In the heating stage, energy transferred to the workpiece as heat input serves as the boundary condition on the top surface AB (Fig. 3). In the cooling stage, radiation and convection heat losses are considered. The boundaries BC and CD are at such distances that there is no heat transfer across them. The boundary AD is an axis of symmetry. Thus the boundary conditions are:

$$-\lambda\frac{\partial T}{\partial z} = \begin{cases} q(r,t) & \text{if } 0 < t \le t_p \\ \beta(T_0 - T) & \text{if } t > t_p \end{cases} \quad \text{on AB}, \tag{2}$$

$$\frac{\partial T}{\partial n} = 0 \quad \text{on BC, CD, AD}, \tag{3}$$

where $q(r,t)$ is the quantity of heat flux entering into the workpiece, t_p is the discharge pulse duration, T_0 is the room temperature, direction n is normal to the boundary and β is the integrated heat transfer coefficient calculated by:

$$\beta = h + \varepsilon\sigma(T + T_0)(T^2 + T_0^2), \tag{4}$$

where h is the free convection coefficient, ε is the surface emissivity, σ is the Stefan−Boltzmann constant.

The initial temperature can be taken as room temperature, that is:

$$T(r,z,0) = T_0 \quad \text{at } t = 0. \tag{5}$$

3.4. *Heat input*

The Gaussian heat input model is well known and well accepted that it has been used in the modeling of electrical discharge machining.[10−12] In this paper, the Gaussian heat input model is used to calculate the heat input during LIDSS. The heat flux $q(r,t)$ at radius r and time t is given by:

$$q(r,t) = kq_0 \exp\left\{-k\left(\frac{r}{R}\right)^2\right\}, \tag{6}$$

$$q_0 = \frac{\eta \cdot Q}{\pi R^2 t}, \tag{7}$$

where q_0 is the average intensity, Q is the total discharge energy of a single discharge, R is the discharge channel radius, k is the energy concentration factor of Gaussian distribution and η is the energy absorption rate of workpiece.

3.4.1. *Discharge channel radius* (R)

The radius of the discharge channel is not a constant. According to Patel,[13] the discharge channel was an expanding quantity and its radius changes with time. Equation (8) obtained by Patel, can be used to calculate the radius in electrical discharge machining process. The empirical constant r_{g0} is equal to 0.788.

$$R(t) = r_{g0}t^{0.75}. \tag{8}$$

Erden[14] showed that the discharge channel is influenced by the discharge power and time. For a rectangular pulse, the following empirical relationship is suggested for the discharge channel radius for selected pairs:

$$R(Q,t) = KQ^m t^n, \tag{9}$$

where Q is discharge power and K, m and n are empirical constants correlated with electrode materials, discharge length and other discharge conditions.

Marafona[10] used Eq. (10) to calculate the discharge radius which is related to the current intensity and pulse duration. The empirical constants K, m and n are equal to 0.00204, 0.43 and 0.44, respectively.

$$R(I,t) = KI^m t^n. \tag{10}$$

3.4.2. *Energy distribution factor* (k)

The energy distribution factor of Gaussian heat input model is used to characterize the centrality of heat flux. The heat flux is more concentrated as the factor is larger (Fig. 4). The value of k is dependent on

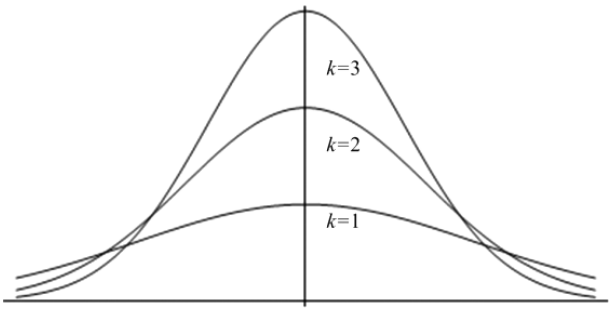

Fig. 4. The energy distribution factor of Gaussian heat input model.

machining conditions, such as the shape of tool electrode. According to Das[11] and Patel,[13] the value of k was set to 1 while set to 4.5 by Joshi[1] and Yadav.[12] No comprehensive method has so far been suggested to calculate the value of k for the Gaussian heat input model.

3.4.3. *Energy absorption rate* (η)

Total discharge energy released in the discharge channel is spent at three places, namely: workpiece, tool electrode and dielectric. The energy absorbed by workpiece is used to heat the material and form the discharge pit over the surface. The material properties of individual workpiece and the machining conditions determine the value of energy absorption rate of workpiece. Patel[13] and DiBitonto[15] used a constant power fraction of 0.08 and 0.183 for the anode and cathode model, respectively. Shankar[2] found that about 40−45% of total power is absorbed by the workpiece during electrical discharge machining.

Since the experimental conditions were varied according to the above authors, the values of R, k and η were not in agreement. So we obtain those values based our experimental conditions which will be discussed in detail later in this paper.

3.5. *Phase transitions*

The temperature changes in the workpiece associated with LIDSS induce change of phase in the material. Regions that achieve the melting temperature are called fusion or molten region. For the molten areas the phase changes from solid to liquid. During melting there is a fraction of material in solid state

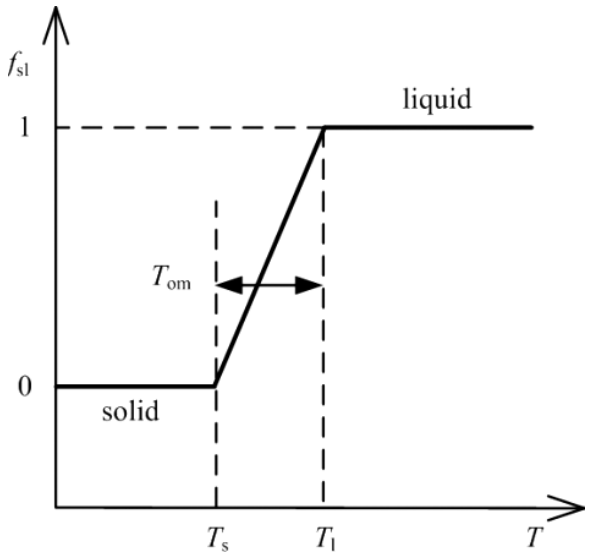

Fig. 5. Graphic of the variable f_{sl} as function of the temperature for the phase transition solid−liquid. For $f_{sl} = 0$, the metal is in solid state and for $f_{sl} = 1$, it is completely molten. The same scheme is applicable for the liquid−vapor transition.

and a fraction in liquid state in molten region. The liquid fraction is represented by the variable f_{sl}. For $f_{sl} = 0$ the metal is in solid state and for $f_{sl} = 1$ it is completely molten (Fig. 5). The fraction f_{sl} changes as a function of temperature as shown:

$$f_{sl} = \begin{cases} 0 & \text{if } T < T_s \\ 1 & \text{if } T > T_l \\ (T - T_s)/T_{om} & \text{if } T_s \le T \le T_l \end{cases}, \qquad (11)$$

where T_s and T_l are respectively the solidus and liquidus temperatures; T_{om} is a temperature range which is selected to be 50 K, and it takes in account, that the phase transitions do not occur instantaneously at a fixed temperature.

The enthalpy function H is defined as the integral of heat capacity with respect to temperature. One has the following general form:

$$H = \int_{T_{ref}}^{T} \rho c \mathrm{d}T, \qquad (12)$$

where T_{ref} is a reference temperature. The form of the function H in Eq. (12) depends highly on the material type considered in the problem. In this paper, the phase change takes place over a finite interval $[T_s, T_l]$, so the enthalpy function (12) can be

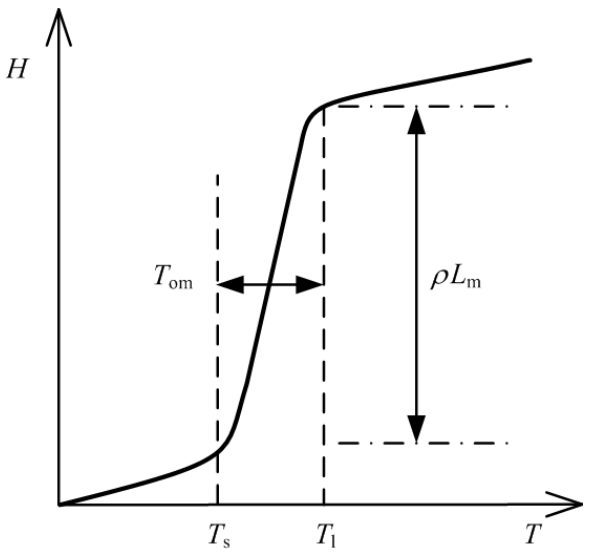

Fig. 6. Typical enthalpy versus temperature relation. ρL_m is the energy required for a unit volume of solid at temperature to be transformed into liquid.

equivalently given by:

$$H = \begin{cases} \int_{T_{ref}}^{T} \rho c \mathrm{d}T & \text{if } T < T_s \\ \int_{T_{ref}}^{T_s} \rho c \mathrm{d}T + f_{sl}\rho L_m & \text{if } T_s \le T \le T_l \\ \int_{T_{ref}}^{T_s} \rho c \mathrm{d}T + \rho L_m + \int_{T_l}^{T} \rho c \mathrm{d}T & \text{if } T > T_l \end{cases}, \tag{13}$$

where L_m denotes the heat of fusion, that is to say, ρL_m is the energy required for a unit volume of solid at temperature to be transformed into liquid (Fig. 6).

The liquid−vapor transition is considered in the same way using the vaporous temperature T_v, the latent heat of vaporization L_b, the variable f_{lv} and the temperature range T_{ob} ($T_{ob} = 300\,\mathrm{K}$).

3.6. *Material properties*

The material properties are temperature-dependent generally. When the temperature range is not significant, average material properties can be used. During the LIDSS a larger temperature range of workpiece is involved. Thus, it is imperative that temperature-dependent material properties be used for the computation process. The 1045 steel properties used in this paper are listed in Table 2.

Table 2. Temperature-dependent properties of 1045 steel.

T (K)	C (J/kg K)	λ (W/m K)	ρ (kg/m^3)
293	472	47.68	7847
473	498	40.44	7800
673	560	36.02	7731
873	700	31.98	7655
1028	1064	25.14	7604
1073	806	26.49	7594
1273	602	24.02	7485
1753	670	24	7330
1803	790	24	7280
2913	830	24	7070
3023	840	24	6980
3213	840	24	6980

During the rapid heating or cooling as electrical discharge machining, material required higher temperature for phase transitions than conventional heat treatment. For carbon steel, this temperature may be approximately 50−300 K higher than the general case.[3] In the current work, the martensitic transformation temperature and solid−liquid transformation temperature are 1173 and 1873 K, respectively.

3.7. *Calculation procedure*

An analytical code is developed to calculate the temperature distribution for LIDSS based on ANSYS Parametric Design Language (Release 12.0). To save the CUP time and improve the computation accuracy, spatial nonuniform grids are introduced. A finer grids spacing is used near the heat source. The computational domain has dimensions of 2 mm in width (r direction) and 1.5 mm in depth (z direction) and the corresponding grid system contains 100×100 grid points. The minimum grid spacing along the r and z directions is about 5 and 2 μm, respectively. The time step used in the heating stage is 0.01 ms while for cooling stage is 0.05 ms.

4. Results and Discussion

4.1. *Factors of Gaussian heat input*

The Gaussian model has three key factors, as discussed above, the discharge channel radius (R), the energy absorption rate of workpiece (η) and the energy distribution factor (k). In this paper, R is calculated

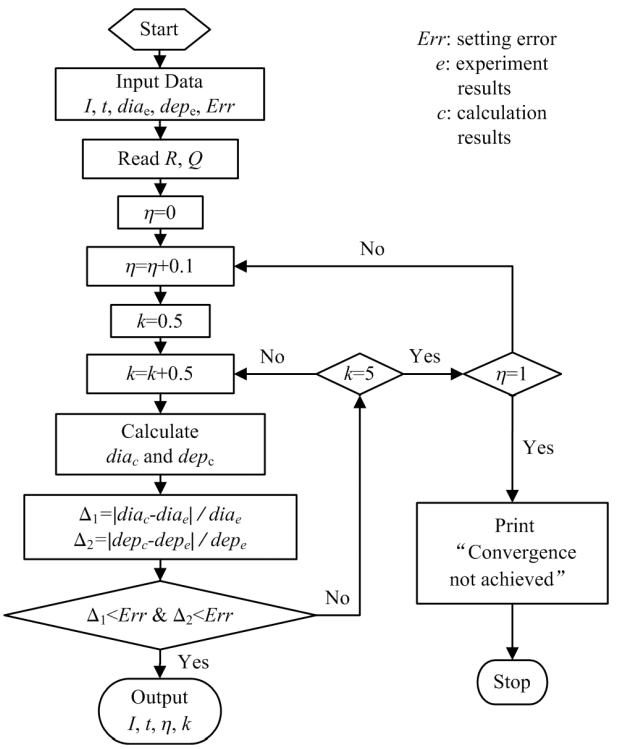

Fig. 7. Flow chart of the program used to obtain the energy absorption rate (η) and the energy distribution factor (k).

based on Eq. (10) suggested by Marafona.[10] The empirical formula for R which is obtained by the least squares fitting is shown as:

$$R = 0.086 I^{0.36} t^{0.25} + r_0, \tag{14}$$

where r_0 is the laser spot radius (mm), I is the discharge current intensity (A) and t is the discharge duration (ms).

The energy absorption rate of workpiece (η) and the energy distribution factor (k) cannot be measured merely with experimental methods. To obtain these values, we develop a program where the above thermal model is applied (Fig. 7). According to literature,[1,11–13] k ranges from 1 to 5 and η from 0 to 1. When the program ends, the following formulas are obtained:

$$\eta = 1.73 I^{-0.42} (t + 0.8)^{0.45}, \tag{15}$$

$$k = 2, \tag{16}$$

where η is a function of I and t, whereas k is a constant and equal to 2. During the LIDSS process, the energy absorption rate η increases with discharge duration, but when the duration is shorter than 0.2 ms, the rate increases slowly and it could be considered as a constant.[2,13,15]

4.2. *Comparison between the calculated and experimental results*

The experimentally determined discharge pit cross-sections are compared with the corresponding calculated values in Fig. 8. It is shown that the computed discharge strengthening pit geometry and dimensions agree well with the experimental results. The calculated values of pit diameter and the depth of hardened layer for various discharge duration and current intensity fit the experimental data well (Fig. 9). The fair agreement indicates validity of the transient axisymmetric thermal model.

4.3. *Temperature fields*

The computed temperature fields as a function of time are shown in Fig. 10(a)–10(d). In the initial period, the molten area expands rapidly in size and the temperatures increase with time. At the end of the discharge pulse, the peak temperature drops and the molten area shrinks rapidly, as shown in Fig. 10(c) and 10(d). The calculations indicate that the molten area resolidifies completely in about 3.9 ms after the discharge pulse is switched off.

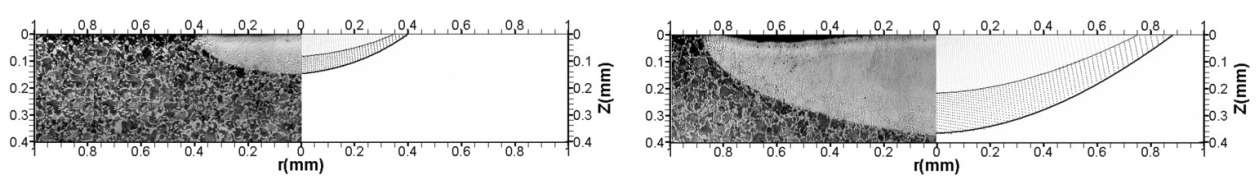

(a) (b)

Fig. 8. Experimental and calculated discharge pit cross-sections for (a) current intensity: 55 A, discharge duration: 1.44 ms, (b) current intensity: 153 A, discharge duration: 6.94 ms.

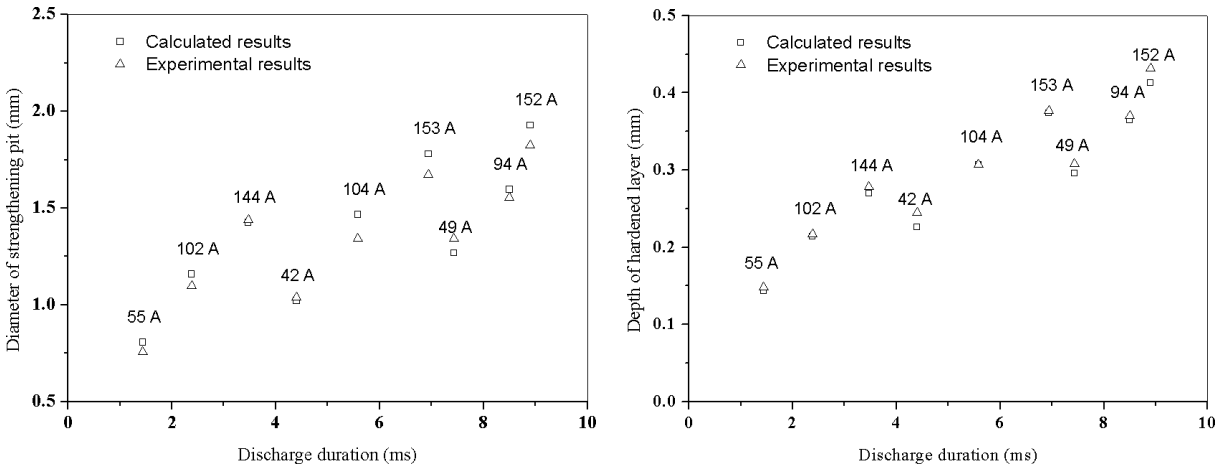

(a) (b)

Fig. 9. The experimental and calculated results of discharge duration and current intensity on (a) the diameter of discharge pit and (b) the depth of hardened layer.

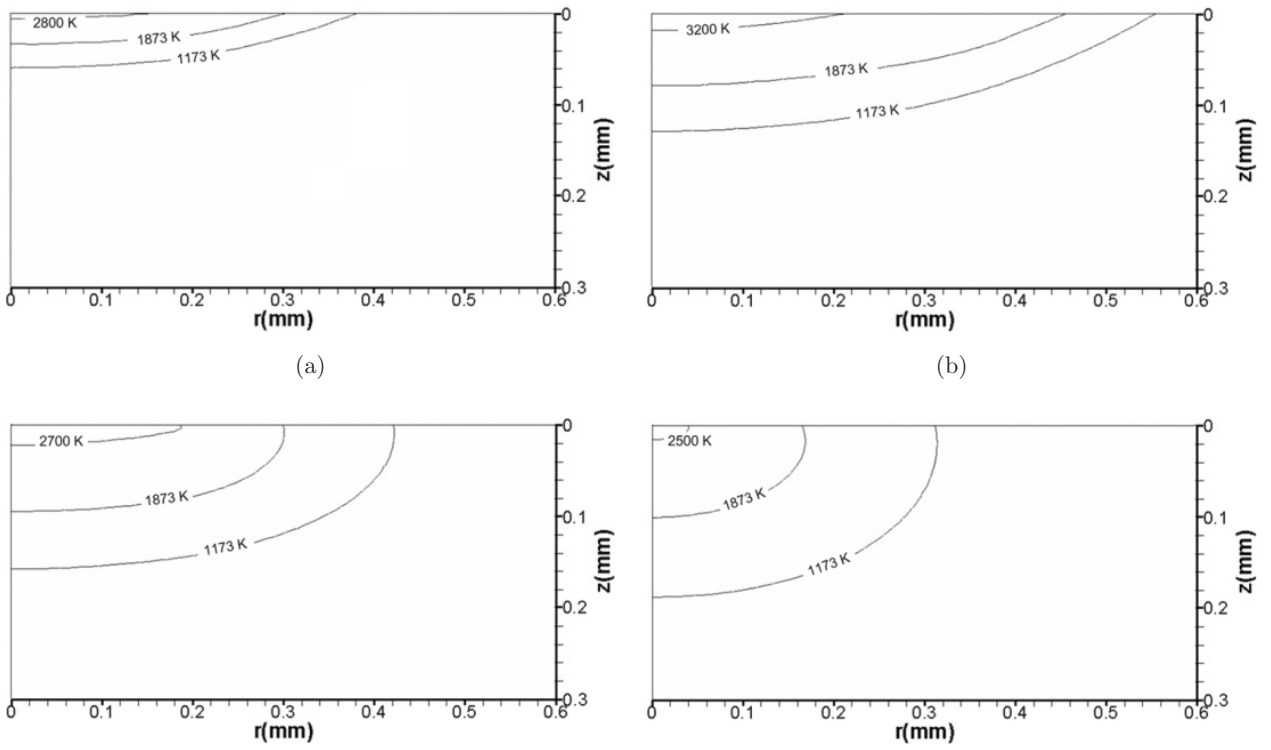

(a) (b)

(c) (d)

Fig. 10. Calculated temperature fields at different times: (a) $t = 0.5$ ms, (b) $t = 2.0$ ms, (c) $t = 3.0$ ms, (d) $t = 5.0$ ms. Current intensity: 200 A and discharge duration: 2 ms.

5. Conclusion

We have described in detail a thermal model that is developed to predict the temperature field of LIDSS process. Based on this model, the temperature field of LIDSS is calculated and the results are well consistent with the experimental data. With the thermal model it is possible to estimate the discharge pit geometry and dimensions as well as the pit diameter

and the depth of the hardened layer for the LIDSS process. The thermal model also can be used to investigate the temperature field due to other surface processing involved Gaussian heat input such as Laser-texturing. The process Laser-texturing analysis is ongoing in our laboratory and will be reported in due course.

Acknowledgments

This work is supported by the National Nature Science Foundation of China under Grant No. 60877064. We thank Mr. Lei Zhang, Mr. Wei Guo and Dr. Xiuli He for their comments on various drafts of this paper.

References

1. S. N. Joshi and S. S. Pande, *Int. J. Adv. Manuf. Technol.* **45** (2009) 300.
2. P. Shankar, V. K. Jain and T. Sundararajan, *Mach. Sci. Technol.* **1**(2) (1997) 195.
3. S. Tariq Jilani and P. C. Pandey, *Precis. Eng.* **4**(4) (1982) 215.
4. K. M. Patel, P. M. Pandey and P. V. Rao, *Int. J. Refract. Met. Hard Mater.* **27** (2009) 892.
5. J. Marafona and C. Wykes, *Int. J. Mach. Tools Manuf.* **40** (2000) 153.
6. Z. Y. Li, M. J. Yang, W. J. Liu and M. L. Zhong, *Surf. Coat. Technol.* **200** (2006) 4493.
7. Z. Y. Li, M. J. Yang, M. L. Zhong and W. J. Liu, *Surf. Rev. Lett.* **13**(4) (2006) 403.
8. Z. T. Wang, J. Zhan and M. J. Yang, *IEEE Trans. Plasma Sci.* **36**(5) (2008) 2816.
9. Z. T. Wang, Z. Q. Zhou, Y. L. Han, M. Shi and M. J. Yang, *IEEE Trans. Plasma Sci.* **38**(4) (2010) 943.
10. J. Marafona and J. A. G. Chousal, *Int. J. Mach. Tools Manuf.* **46** (2006) 595.
11. S. Das, M. Klotz and F. Klocke, *J. Mater. Process. Technol.* **142** (2003) 434.
12. V. Yadav, V. K. Jain and P. M. Dixit, *Int. J. Mach. Tools Manuf.* **42** (2002) 877.
13. M. R. Patel, M. A. Barrufet, P. T. Eubank and D. D. DiBitonto, *J. Appl. Phys.* **66**(9) (1989) 4104.
14. A. Erden, *J. Eng. Mater.Technol.* **105** (1983) 132.
15. D. D. DiBitonto, P. T. Eubank, M. R. Patel and M. A. Barrufet, *J. Appl. Phys.* **66**(9) (1989) 4095.